



# A Large-Scale Application of the Stochastic Approach for Estimating the Shear Strength of Natural Rock Discontinuities

M. Jeffery<sup>1</sup> · J. Huang<sup>1</sup> · S. Fityus<sup>1</sup> · A. Giacomini<sup>1</sup> · O. Buzzi<sup>1</sup>

Received: 30 October 2022 / Accepted: 16 May 2023 / Published online: 30 May 2023  
© The Author(s) 2023

## Abstract

Reliable shear strength determination of large in situ discontinuities is still a challenge faced by the rock mechanics field. This is principally due to the limited availability of surface roughness and morphology information of in situ discontinuities and the unresolved management of the ‘scale effect’ phenomenon. Recently, a stochastic approach for predicting the shear strength of large-scale discontinuities was established, encompassing random field theory, a semi-analytical shear strength model, and a stochastic analysis framework. A key aspect of the new approach is the application at field scale, thereby minimising or bypassing the scale effect. The approach has been validated at laboratory scale and an initial large-scale deterministic-based validation showed promising results. However, to date, no large-scale experimental-based validation has been undertaken. This paper presents the first rigorous application of the employed semi-analytical shear strength model and the stochastic approach on a 2 m-by-2 m discontinuity surface, with comparison of prediction to experimental shear strength data. The shear strength model was found to generally produce peak and residual predictions within a  $\pm 10\%$  relative error range, with good agreement between predicted and observed damage areas. It was observed that, applying the stochastic approach to seed traces with gradient statistics equivalent to that of the surface, produced predictions that closely resemble the experimental results. Whereas, predicting shear strength from different seed traces results in more variability of predictions, with many falling within  $\pm 20\%$  of the experimental data. The predictions of residual shear strength tended to be more accurate than peak shear strength.

## Highlights

- The stochastic approach for discontinuity shear strength was applied to a 2 m per 2 m rock surface replica made of mortar.
- A sensitivity analysis conducted on the analytical shear strength model highlights the parameter influencing the most the shear strength prediction.
- The predictions of peak and residual strengths fall within 20% of the experimental data.
- The accuracy of prediction depends on the trace used to define the input statistics.

**Keywords** Rock joint · Discontinuity · Large scale · Shear strength · Scale effect · Stochastic

## 1 Introduction

The shear strength of large discontinuities is an important parameter in stability assessment of rock slopes, especially where infrastructure, operations, and/or human life may be

at risk. However, estimating shear strength for large in situ discontinuities is challenging due to the limited visible morphological and roughness features of the surface, and the non-trivial and generally prohibitive nature of large-scale experiments (Casagrande et al. 2018). Due to these challenges and a lack of alternative options, researchers and practitioners either test laboratory-sized samples and/or employ empirical methods for estimating shear strength of large discontinuities. This in turn introduces another challenge, accounting for change of scale. Indeed, small-scale predictions are not directly applicable at the project scale

✉ O. Buzzi  
Olivier.Buzzi@newcastle.edu.au

<sup>1</sup> Priority Research Centre for Geotechnical Science and Engineering, University of Newcastle, Callaghan, NSW 2208, Australia

but rather require an adjustment to account for the increase in scale, which is commonly referred to as “scale effect” (Barton and Bandis 1980).

The effects of scale on discontinuity roughness, shear strength, and deformability have been continually studied since the 1960s. The agreement that scale matters and advancements in testing apparatuses has facilitated various efforts to resolve our understanding of the scale effect and develop strategies to account for scale when estimating large-scale shear strength. However, conflicting observations and conclusions have been published. Researchers have observed or reported positive, negative, or no scale effects (Barton and Bandis 1980; Pratt et al. 1972; Muralha and Pinto da Cunha 1990a, 1990b; Ohnishi and Yoshinaka 1995; Kutter and Otto 1990; Leal Gomes 2003; Johansson 2016). The complexity of capturing the scale effect stems from the multiscale nature of surface roughness, a key factor influencing shear strength (Hencher et al. 1993; Barton and Choubey 1977; Maerz et al. 1990).

In practise, estimations of large-scale shear strength are typically derived from a small amount of roughness information relative to the full surface and rely on an assumption that this limited information is representative (either morphologically and/or statistically) of the whole surface. If this assumption is incorrect or overlooked, it is important to have an understanding of the variability that may be introduced and how this will influence shear strength estimations (Fardin et al. 2001; Buzzi et al. 2017).

Despite years of research, leading to significant advancements in the characterisation, understanding, and modelling of mechanical response of discontinuities, the scale effect still remains not fully understood and modelled. As it is difficult to determine the degree of scaling required, there is continued uncertainty towards an appropriate strategy to resolve the upscaling from small shear strength (Giani et al. 1995).

In practise, there are few methods for estimating the shear strength of large discontinuities. Versions of empirical JRC shear strength model modified to incorporate scale changes (Barton and Bandis 1982; Barton 1982) are commonly adopted. However, aspects of its implementation have raised concerns, most notably Barton (2013) commented that the JRC shear strength model is commonly incorrectly applied. Beer et al. (2002) showed that visually estimating JRC values via comparisons with the standardised JRC profiles can be a subjective process producing inconsistent results. Barton et al. (2023) recently stated that the JRC should capture the 3D morphology of a joint and its directional shear response, which can be achieved by back analysing JRC from tilt tests, and that JRC should not be seen as only reflecting 2D roughness.

Alternatively, back analysis techniques and observations of large discontinuity failures have been used to estimate

various design parameters, such as Mohr–Coulomb parameters (apparent cohesion  $c$  and friction angle  $\phi$ ), first-order roughness inclination angles, JRC values, and/or other friction angle parameters (basic,  $\phi_b$ , and ultimate/residual  $\phi_u/\phi_r$ ) (Barton 1971; Kim et al. 2014; Amarasekera 2015; Markov et al. 2019), which can then be used to inform and guide future designs and stability assessments for similar discontinuities in the same location. Whilst providing insightful observations and design information, back analysis techniques require a failure to have occurred, which is typically not acceptable in many situations.

In recent years, a new stochastic philosophy and methodology has been proposed for estimating large-scale discontinuities shear strength (Casagrande et al. 2018; Buzzi et al. 2017; Buzzi and Casagrande 2018). Referred to in this paper as the Stochastic Approach for Discontinuity Shear Strength (STADSS), it offers a shift from conventional deterministic methods to rigorous stochastic analyses.

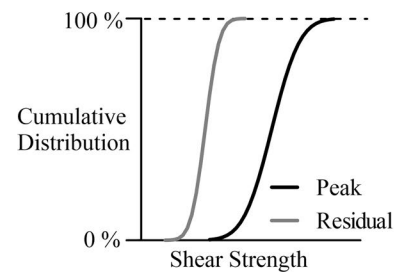
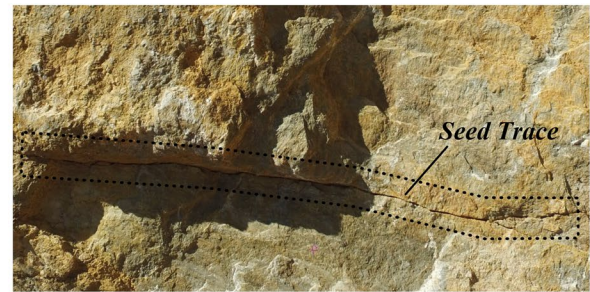
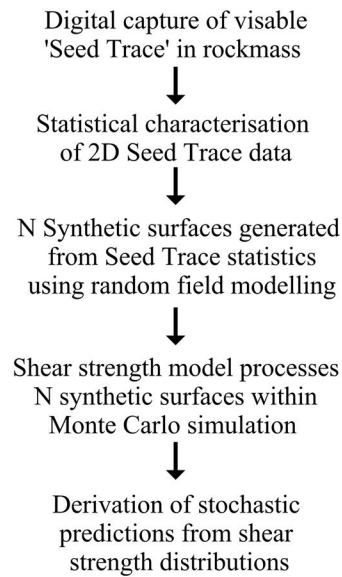
The STADSS relies on two key components: (1) a random field model for producing 3D synthetic rough surfaces with controlled statistics from the statistics of a seed trace (2D profile of a discontinuity daylighting at the rock face), and (2) a semi-analytical shear strength model capable of predicting the peak and residual shear strength of 3D synthetic surfaces, given a shear direction, a normal stress, and material strength properties. By predicting the shear strength of all synthetic surfaces, STADSS produces a distribution of peak and residual shear strength and, because it is applicable at problem scale, it can bypass potential scale effect issues. The key steps of the STADSS are illustrated in Fig. 1, after Casagrande et al. (2018).

Buzzi and Casagrande (2018) applied the STADSS to a 2 m per 2 m natural surface but could not compare the STADSS prediction to experimental data and several issues were identified. Nonetheless, the preliminary results were encouraging.

This paper presents the first rigorous application of the STADSS to a large (2 m per 2 m) rock discontinuity surface where STADSS predictions are compared to experimental values of shear strength. For this study, the computationally efficient semi-analytical shear model, presented in Casagrande et al. (2018) (referred to here as the Newcastle Discontinuity Shear Strength (NDSS) model), was coupled with the multiscale approach for generating large-scale rough rock surfaces established by Jeffery et al. (2021). The experimental data were obtained on 2 m per 2 m discontinuity replicas tested under initial normal stresses ranging from 5 to 31 kPa; for details pertaining to the creation of the 2 m PER 2 m surface replicas and very large direct shearing apparatus, refer to Jeffery et al. (2022).

The first part of the paper explores the reliability of the NDSS predictions at large scale, by comparing deterministic predictions to experimental results. The second part of the

**Fig. 1** Overview of the steps in the STADSS for estimating shear strength of large in situ discontinuities (after Casagrande et al. 2018)



paper deals with the application the STADSS to the large surface with a focus on selection of seed traces, comparison of stochastic predictions and experimental shear strength, and, finally, limitations and uncertainties of the approach. This is the first time the NDSS model and STADSS have been compared to experimental data at large scale, hence offering a first step towards validation of the STADSS.

## 2 Characteristics of the Surface and Replicas Tested

### 2.1 Material Characterisation

The surface replicas were cast using a mortar mix comprising of a 4:2:1 ratio of sand, cement, and water. Due to the high cement ratio, several admixtures (superplasticiser, water reducer, and retarder) were incorporated into the mix to assist with placement into the moulds. Once cast, the replicas were cured for 7 weeks (Jeffery et al. 2022).

The NDSS model can use either Mohr–Coulomb ( $c$  and  $\phi$ ) or Hoek–Brown ( $\sigma_{ci}$  and  $m_i$ ) and a basic friction angle,  $\phi_b$ , parameters to describe the material strength properties. For this research, the mortar material strength was characterised in terms of the Hoek–Brown parameters,  $\sigma_{ci}$  and  $m_i$ , which were estimated using unconfined compression strength tests (15 tests) and triaxial tests (utilising a Hoek cell, 20 tests) as per ISRM suggested methods (International Society of Rock Mechanics, 1983). The triaxial compression tests were conducted under confinement stresses (minor principal stresses,  $\sigma_3$ ) of 10, 20, 30, and 40 MPa. Note that these stress values are much larger than the normal stress to be applied to the discontinuity (up to 31 kPa), but it is essential to capture

the effect of localised stress concentration developing in a sheared discontinuity. With less than 1% of the surface in contact during shearing (Jeffery et al. 2022), the local normal stress is multiplied by a factor 100 or more. Characterising material strength under a normal stress equivalent to the “average” normal stress acting on the whole surface is likely to result in an inadequate estimate of the failure criterion, especially for a non-linear strength envelope.

The mortar cylinders used for the compressive strength testing were cored from each surface replica and trimmed to a length-to-diameter ratio of 2.5:1. Estimation of the material’s basic friction angle,  $\phi_b$ , was achieved from direct shear tests (using a Geocomp ShearTrac II direct shear box), following revised ISRM suggested methods (Muralha et al. 2013). In total, 16 direct shear tests were conducted on 100 mm × 100 mm planar mortar surfaces, tested under constant normal stress conditions for normal stresses of 20, 50, 100, and 250 kPa. Figure 2 presents a summary of the material characterisation data and determination of the mortar material parameters. Table 1 reports the results of material characterisation.

### 2.2 Morphology and Statistics of the Whole Surface

The surface of the bottom wall replicate (Fig. 3a) was digitally reconstructed prior to shearing using photogrammetric methods and 29 ground control points (GCP), setup around (16 of 29 GCP), and on the surfaces (13 of 29 GCP). The local spatial positions ( $x, y, z$ ) of the ground control points were surveyed using a theodolite (Leica MS60 total station) and were utilised as spatial control points in the imagery reconstruction process. Using a Nikon D850 DSLR camera with a 24 mm lens, 100 photos were taken of the surface

**Fig. 2** Experimental results and characterisation of the mortar material; **a** unconfined and tri-axial compressive strength tests results (grey circles) plotted in terms of major principal stress ( $\sigma_1$ ) as a function of minor principal stress ( $\sigma_3$ ); **b** residual shear strength as a function of normal stress obtained by direct shear tests on flat mortar surfaces (Color figure online)

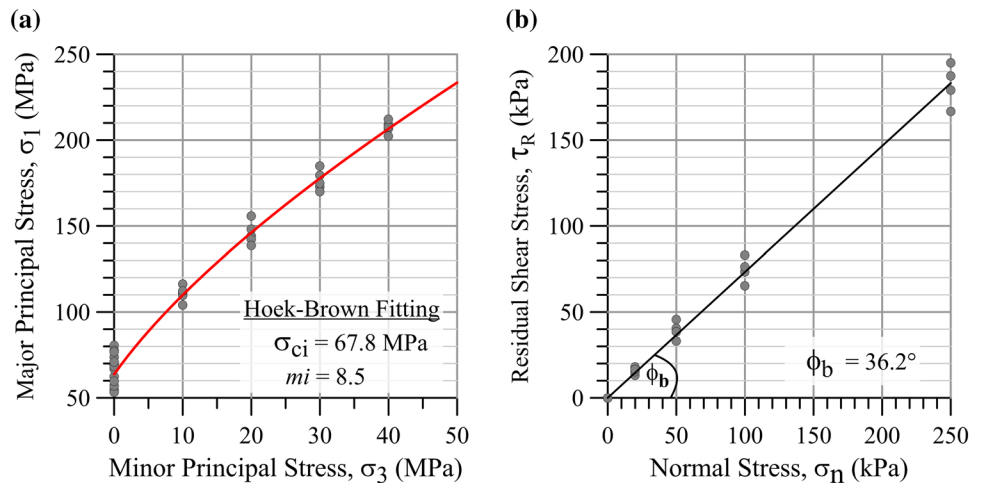


**Table 1** Material strength parameters for the mortar used to cast the surface replicas; unconfined compressive strength,  $\sigma_c$  Hoek–Brown intact material parameters,  $\sigma_{ci}$  and  $m_i$  and basic friction angle,  $\phi_b$

Unconfined compressive strength $\sigma_c$ (MPa)	Hoek–Brown intact parameters		Basic friction angle, $\phi_b$ (°)
	Unconfined compressive strength $\sigma_{ci}$ (MPa)	$m_i$	
Mean: 68.0 stdev: 8.8	67.8	8.5	Mean: 36.2 stdev: 2.3

from multiple perspectives. Using Agisoft Metashape, the surface was modelled as a 3D point cloud with average reconstruction  $x$ ,  $y$ , and  $z$  spatial errors of 560  $\mu\text{m}$ , 720  $\mu\text{m}$ , and 430  $\mu\text{m}$ , respectively. For numerical and mapping purposes, the point cloud data were transformed into a 1 mm resolution gridded structure of points with  $x$ ,  $y$ , and  $z$  coordinates using the mapping software package Surfer 13. The 3D contoured representations of the bottom experimental surfaces overlaid with 5 mm contours are presented in Fig. 3b.

The first step of the application of the STADSS to any surface is to statistically characterise the input information. The asperity points of the 3D digital surface model were statistically analysed to obtain the distribution of the asperity heights ( $z$ ) and directional gradients between adjacent points (at a 1 mm increment along  $X$  and  $Y$ ) in both  $X$  and  $Y$  directions.

Casagrande et al. (2018), Buzzi and Casagrande (2018), and Jeffery et al. (2021) characterised many discontinuity surfaces for which the distribution of asperity height did not follow any recognised distribution. Therefore, it is surprising to notice that the distribution of asperity heights of the experimental surface selected for this study resembles a Gaussian distribution (Fig. 3c). Both gradient distributions (Fig. 3d and e) tend to follow Gaussian distributions, which is consistent with observations made by Casagrande

et al. (2018), Buzzi and Casagrande (2018), and Jeffery et al. (2021).

### 2.3 Statistics of Selected Seed Traces

Casagrande et al. (2018) recognised that all STADSS predictions of shear strength are influenced by the statistics of the seed trace. As the seed trace statistics are influenced by the morphological features and roughness textures the trace transects across, it is hence relevant to investigate the variability of input statistics across the study surface.

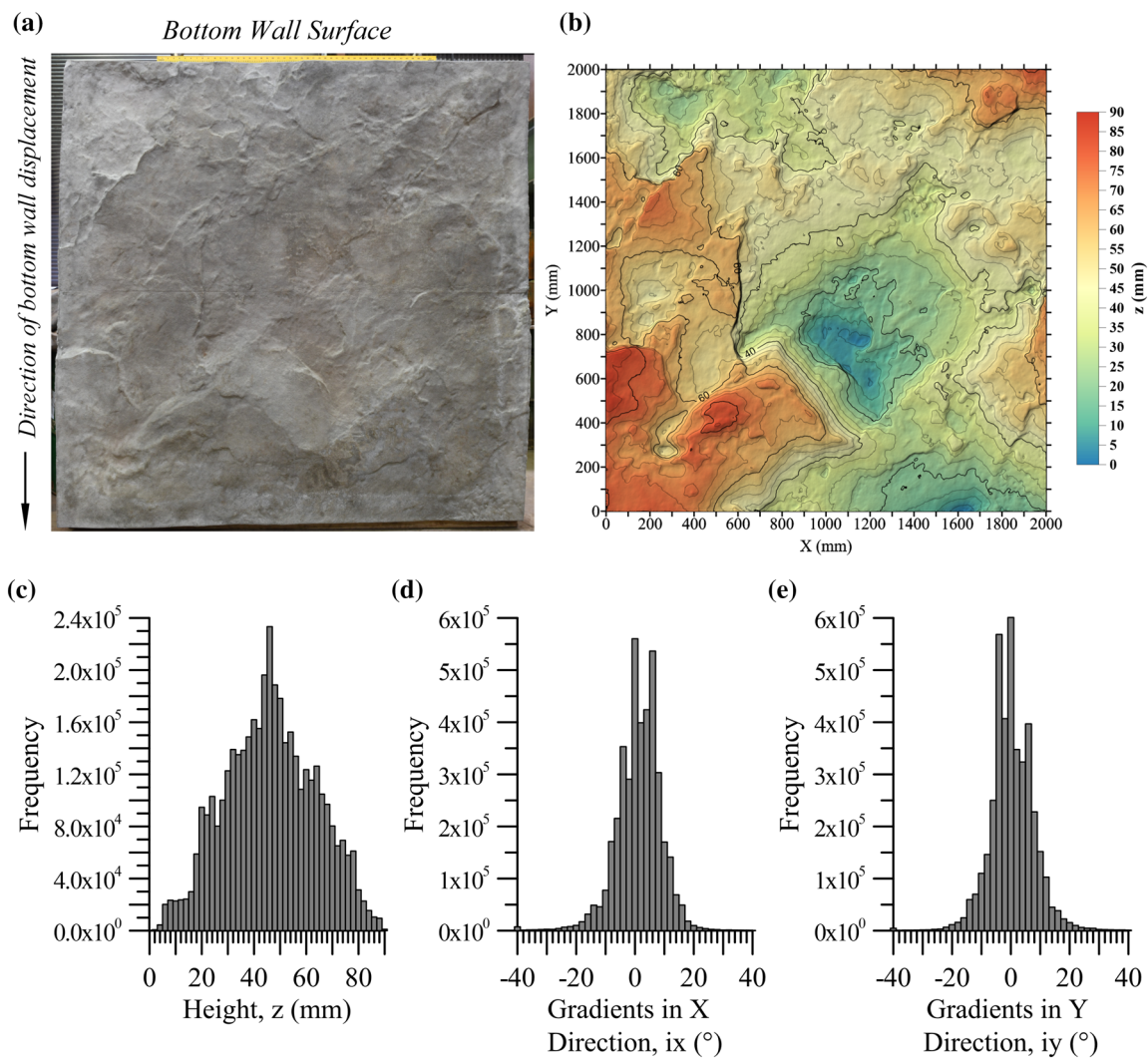
The discretised surface is made of a series of adjacent traces oriented along  $X$  (at constant  $Y$  value) and of adjacent traces oriented along  $Y$  (at constant  $X$  value). A trace with a constant  $X$  value is referred to as an  $X$  trace. The same concept applies to  $Y$ . For each  $X$  and  $Y$  trace (made of 2001 points, 1 mm increment over 2 m distance), the mean and standard deviation of heights and gradients ( $\mu_z$ ,  $\mu_i$ ,  $\sigma_z$ , and  $\sigma_i$ ) is calculated and their evolution as a function of the position of the trace (along  $X$  and  $Y$  axis) is reported in Fig. 4a–d.

Figure 4a–d reveals a significant variability of statistics, from trace to trace, which is expected given observations of Casagrande et al. (2018), Buzzi and Casagrande (2018) and Jeffery et al. (2021). Figure 4d and Figs. 5a and b show that, whilst the maximum standard deviation of gradient is similar in both directions (approximately  $10.6^\circ$ ), the range is slightly wider in the  $Y$  direction (by approximately  $1^\circ$ ) than for the  $X$  direction. The influence and implications of seed trace variability on shear strength predictions is explored in a later section.

Here, a total of 16 seed traces were selected, both in  $X$  and  $Y$  directions:

- Along  $X$ : five traces were chosen in the direction of shearing. Given the narrow distribution of  $\sigma_z$ , traces X1–X4 were chosen to cover a wide range of  $\sigma_i$ . In addition,





**Fig. 3** **a** Photograph of the bottom experimental surface prior to shearing (after Jeffery et al. 2022); **b** 3D digital representation of the bottom experimental surface using Surfer 13, overlain with 5 mm

contours; **c**, **d** and **e** histograms of asperity heights and gradients in the X and Y direction, respectively

a trace that possesses statistics equivalent to the average trace statistics in the X direction was considered (trace identified as AvX).

- Along Y: Four traces (noted Y2, Y4, Y5, and Y6) were selected to capture the full range of  $\sigma_i$ ; five traces (noted Y1, Y3, Y8, and Y9) were selected with a common  $\sigma_i$  (of about  $8^\circ$ ), but with various  $\sigma_z$  to investigate the influence of  $\sigma_z$  (at constant  $\sigma_i$ ) on the shear strength predictions. Additionally, two traces possessing the statistics of the average trace statistics in the Y direction (noted AvY) and of the whole surface (noted WSE) were selected.

The selected traces are presented in Fig. 5a–c together with the evolution of  $\sigma_i$  with  $\sigma_z$  along both directions. The statistics of the selected traces in the X and Y directions are provided in Tables 2 and 3.

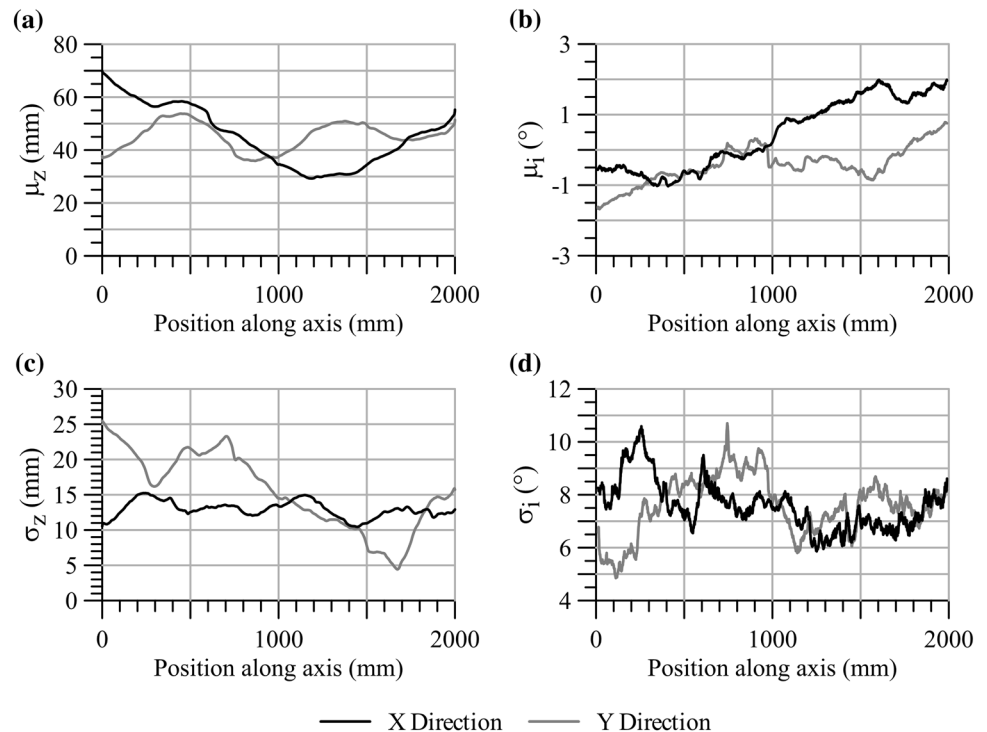
### 3 Results

#### 3.1 Deterministic Prediction of Peak and Residual Shear Strength

The predictive ability of the NDSS model at large scale was first tested by comparing predicted peak and residual shear strength of the surface in Fig. 6 to the experimental results obtained by Jeffery et al. (2022) (reproduced in Fig. 6). The NDSS deterministic predictions were obtained for four initial normal stresses (5, 14, 22, and 31 kPa) using the material parameters presented in Table 1 and shearing direction orientation as per Fig. 3a.

Figure 6 compares the deterministic prediction and the experimental values of peak and residual shear strength, obtained under four initial normal stresses. The black solid

**Fig. 4** Asperity statistics of each trace as a function of their position along the axis; **a** mean height  $\sigma_z$ , **b** mean gradients  $\mu_i$ , **c** standard deviation of height  $\sigma_z$  and **d** standard deviation of gradients  $\sigma_i$ . X and Y direction traces represented by black and grey continuous lines, respectively



line has a gradient of 1:1, whilst the red dashed lines represent a relative prediction error of  $\pm 10\%$ . The predicted shear strength, both peak and residual, are in good agreement with the experimental values, which shows an excellent predictive ability of the NDSS model. The maximum relative error is  $-17\%$ , but, for most predictions, the relative error is lower than  $\pm 10\%$ .

The NDSS model produces a post-shearing surface (as shown in Casagrande et al. (2018)), highlighting the degradation incurred at peak shear strength. Figure 7 compares the post-shearing degradation of the experimental surface (tested under an initial normal stress of 31 kPa) alongside the predicted degradation produced by the NDSS model under the same testing conditions (right and left, respectively).

The first observation is that, in both cases (prediction and experimental), the degraded areas are few and small. These degraded areas reflect the localised interaction of both walls upon shearing and correspond to features with steep inclines, such as steps and/or localised bumps. Although all predicted sheared areas can be found on the real sheared surface (zones circled in red), the damage is more extensive on the experimental surface (Fig. 7b), because damage is not only generated at the peak shear stress but also during the residual phase of shearing. This latter damage mechanism is not captured in the NDSS model, which focuses only on degradation under peak stress.

### 3.2 Sensitivity Analysis of the NDSS Model

The accuracy of the NDSS shear strength predictions relies on the use of adequate material parameters. To explore how sensitive the NDSS model is to each of the key strength parameters ( $\sigma_{ci}$ ,  $m_i$  and  $\phi_b$ ), a parametric study was undertaken.

For each parameter, a series of deterministic peak and residual shear strength prediction were obtained using a range of values, whilst the other two parameters were kept constant (and equal to the values reported in Table 1). For the parametric study:

- The magnitude of unconfined compressive strength  $\sigma_{ci}$  ranged from 50 to 100 MPa, which corresponds to the ISRM field estimate strength classification<sup>32</sup> of *R4* ‘Strong Rock’.
- The range of  $m_i$  explored includes values from 5 to 30, which covers estimates for different rock types, as presented by Hoek and Brown (1997).
- Finally, the basic friction angle was varied from 20 to 40, which covers the basic friction angle of sedimentary, igneous, and metamorphic rocks (Barton 1973, 1976; Alejano et al. 2012).

The results of the NDSS sensitivity parametric study are presented in Fig. 8, which shows the value of predicted peak and residual shear strength as a function of each parameter

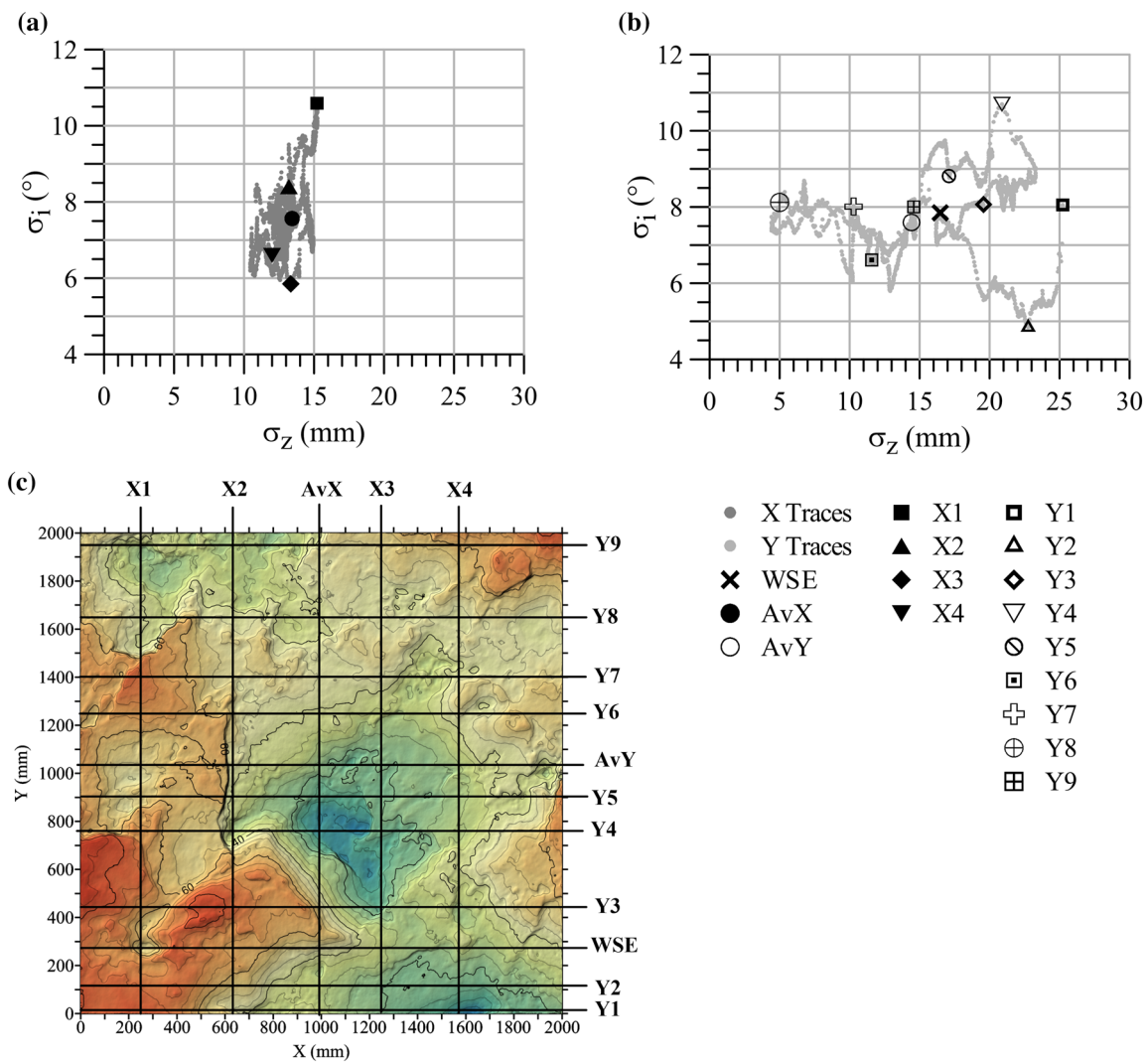


**Fig. 5** **a** Values of standard deviation of gradients  $\sigma_i$  vs. standard deviation of heights  $\sigma_z$  for all traces in the X direction. Each grey dot represents a trace. The selected traces in the X direction are represented by black symbols. **b** Values of standard deviation of gradients  $\sigma_i$  vs. standard deviation of heights  $\sigma_z$  for all traces in the Y direction.

Each grey dot represents a trace. The selected traces in the X direction are represented by hollow symbols. **c** Contoured map of the digitised bottom surface with selected seed traces superimposed (Color figure online)

**Table 2** Statistics of selected seed traces in the X direction

Trace	X1	X2	X3	X4	AvX
X position(mm)	257	633	1251	1571	997
$\sigma_z$ (mm)	15.2	13.2	13.3	12.0	13.4
$\mu_z$ (mm)	23.4	49.2	30.0	37.2	34.5
$\sigma_i$ ( $^\circ$ )	10.59	8.41	5.86	6.60	7.57
$\mu_i$ (mm)	- 0.63	- 0.48	1.01	1.81	0.19

( $\sigma_{ci}$ ,  $m_i$  and  $\phi_b$ ). On each sub-figure, four curves are drawn, corresponding to four values of initial normal stress.

Figure 8a and d shows that changing  $\sigma_{ci}$  only has a minor effect on the strength predictions. Indeed, increasing  $\sigma_{ci}$  from

50 to 100 MPa results in an average maximum increase of peak and residual shear strength by a factor 1.1 and 1.1, respectively.

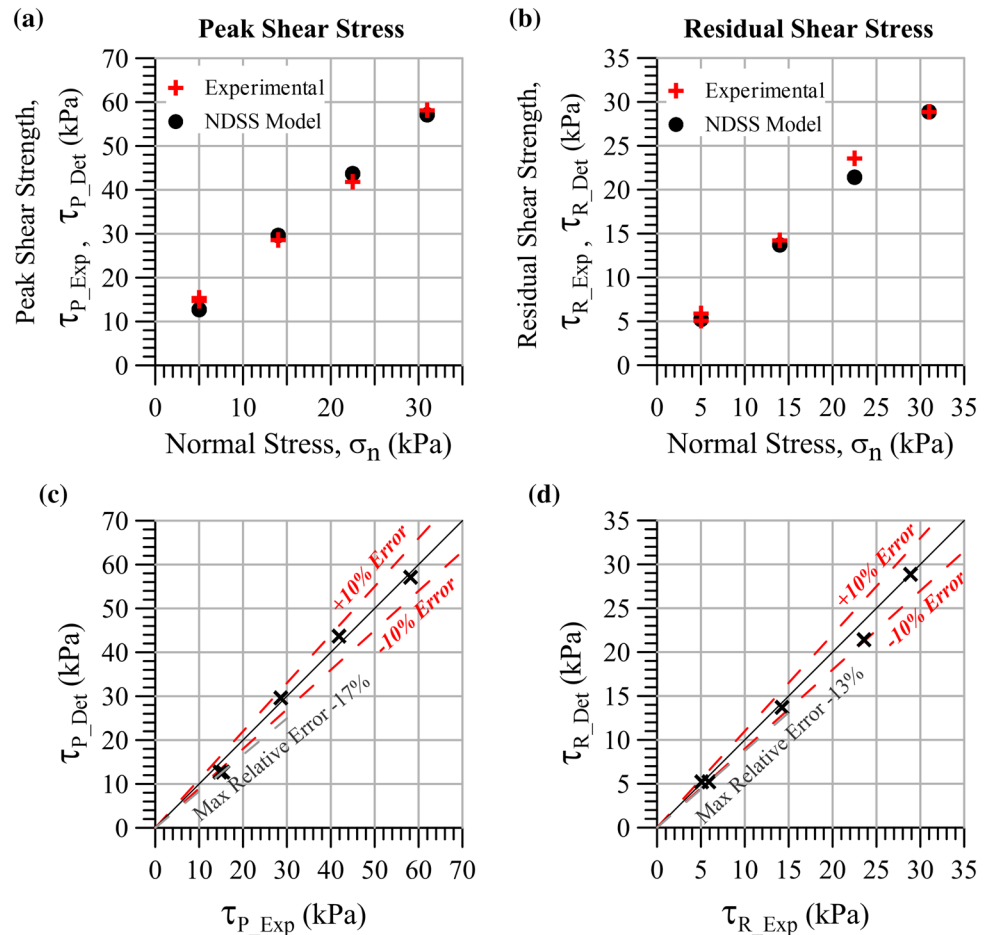
Figure 8b and e shows that  $m_i$  has a marginal effect of the predicted peak shear strength but a strong influence on the predicted residual shear strength. Under all four normal stresses considered, the residual shear strength approximately doubles as  $m_i$  increases from 5 to 30.

Finally, Fig. 8c and f shows that  $\phi_b$  has a more influence on the peak shear strength than on the residual shear strength predictions. When the base friction angle increases from 20 $^\circ$  to 40 $^\circ$ , the peak shear strength increases by a factor 1.8 (on average), whilst the residual shear strength only increases by a factor 1.3 (on average).

**Table 3** Statistics of selected seed traces in the Y direction

Trace	Y1	Y2	Y3	Y4	Y5	Y6	Y7	Y8	Y9	AvY	WSE
Y position (mm)	8	112	414	744	901	1248	1409	1651	1957	1050	279
$\sigma_z$ (mm)	25.2	22.7	19.6	20.9	17.1	11.6	10.3	5.0	14.6	14.4	16.5
$\mu_z$ (mm)	37.1	41.2	53.3	39.6	36.5	48.7	50.4	44.4	46.9	39.4	48.5
$\sigma_i$ (°)	8.06	4.85	8.07	10.70	8.81	6.61	8.01	8.13	8.00	7.60	7.86
$\mu_i$ (mm)	-1.64	-1.38	-0.71	0.18	0.32	-0.33	-0.52	-0.32	0.64	-0.42	-0.97

**Fig. 6** Evolution of measured and predicted shear strength as a function of normal stress: peak (a) and residual (b). Comparison of NDSS deterministic predicted shear strength and experimental shear strength at peak (c) and residual state (d). The continuous black line has a gradient of 1:1, red dashed lines indicate a  $\pm 10\%$  relative error, and grey dashed lines provide maximum value of relative error.  $\tau_{P\_Exp}$ : peak experimental shear strength;  $\tau_{R\_Exp}$ : residual experimental shear strength;  $\tau_{P\_Det}$ : peak deterministic shear strength;  $\tau_{R\_Det}$ : residual deterministic shear strength (after Jeffery et al. (2022)) (Color figure online)



The observed influences can be explained by the shearing mechanics implemented in the NDSS model:

- The peak shear strength is computed from the sliding resistance of all sheared asperities, which is governed by  $\phi_b$ ,  $\sigma_{ci}$  and  $m_i$  are strength parameters used to assess whether active asperities are sheared or not, and to terminate the shearing iterations. Although  $\sigma_{ci}$  and  $m_i$  affects the progressive shearing process and mechanical equilibrium, they are not used to compute the values of peak shear strength, which is why its influence on peak shear strength is only minor.
- The residual shear strength is computed from the peak shear strength (influenced by  $\phi_b$ ), from which a cohe-

sion force (obtained from  $m_i$ ) is subtracted, which is why the residual shear strength is strongly affected by  $m_i$  and, to some extent, by  $\phi_b$ .

The sensitivity analysis was conducted by varying one parameter at a time and with ranges of parameters which wider than those observed in Table 1.

Consequently, to assess how the measured variability of the strength parameters (reflected by the standard deviation of Table 1) affects the prediction, two series of deterministic shear strength predictions were performed. An upper bound prediction was achieved with values of  $\sigma_{ci}$ ,  $m_i$  and  $\phi_b$  equal to the estimated mean value plus one standard deviation (76.6 MPa, 8.5 and 37.6°, respectively), whilst a lower



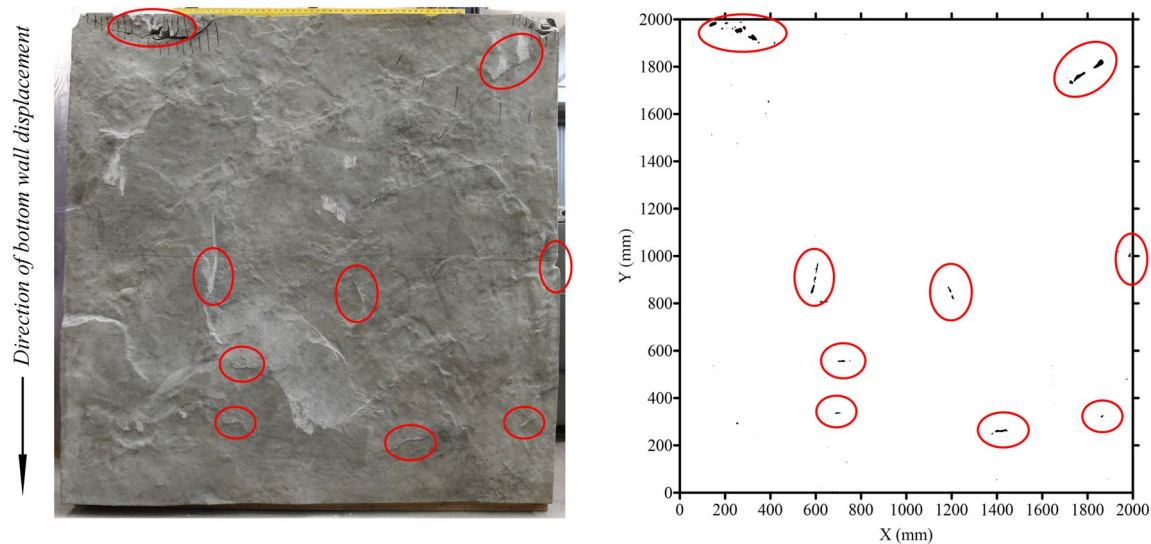


**Fig. 7** Comparison of experimental (left) and NDSS model predicted (right) shear-induced surface degradation under an initial normal stress of 31 kPa. Matching damage zones are highlighted by red continuous circles (Color figure online)

bound series had for input the mean value minus one standard deviation (59.0 MPa, 8.5 and 34.8°, respectively).

Figure 9 compares the predicted upper bound and lower bound to the experimental values of peak shear stress (a) and residual (b). The figure also provides an indication of relative error ( $\pm 10\%$  dashed lines). Given the variability of inputs considered, the range between upper and lower bound is quite narrow for all simulations conducted. Also, most predictions fall within a  $\pm 10\%$  band. The maximum prediction errors are  $-20\%$  and  $+18\%$  for the peak and residual shear strength, respectively.

### 3.3 Statistics of the Randomly Generated Synthetic Surfaces

In line with recommendations by Casagrande et al. (2018), 100 synthetic surfaces were generated for each seed trace, using the multiscale random field model developed by Jeffery et al. (2021). For conciseness, details pertaining to spatial increment length used to decouple the roughness and all random field modelling parameters are presented in Appendix A (Tables 4 and 5, respectively).

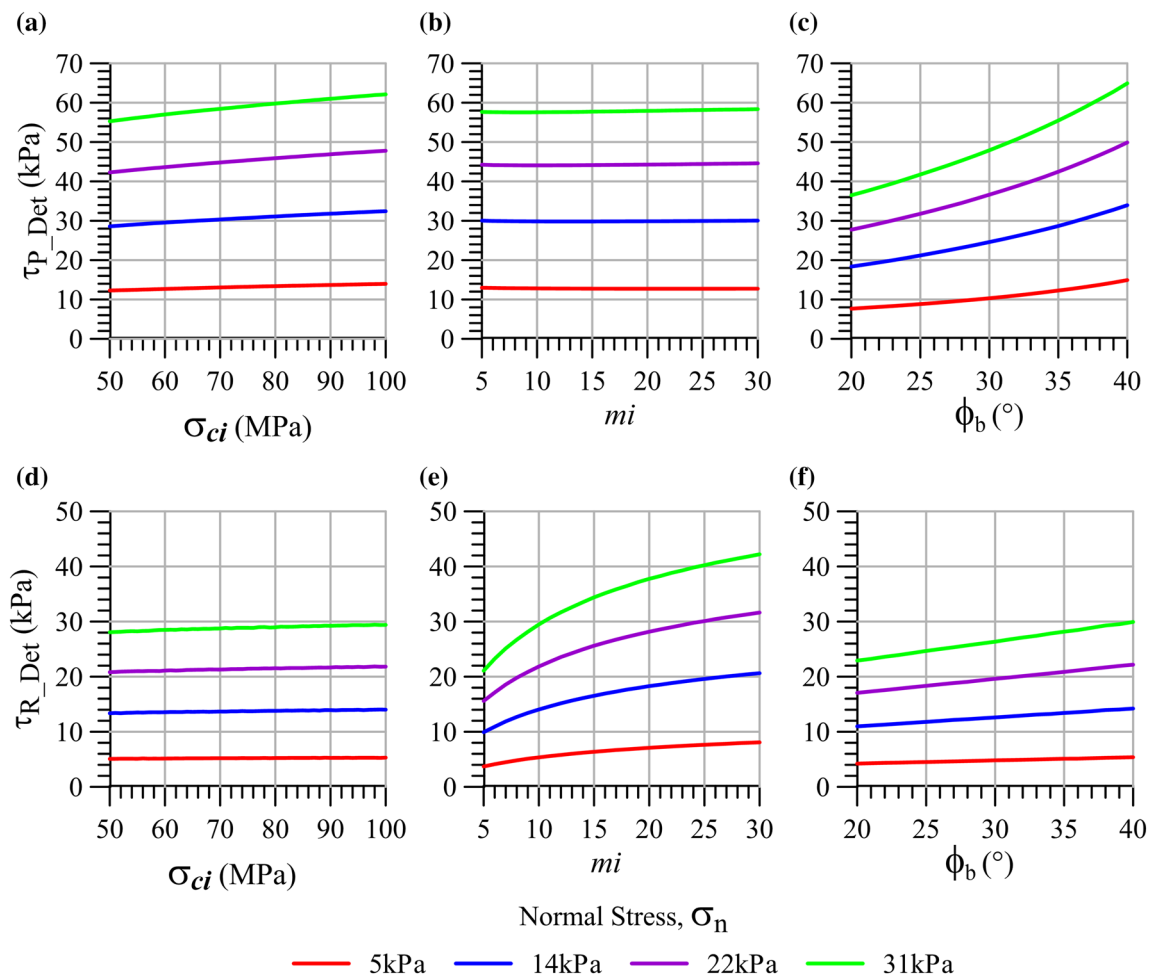
Figure 10 presents the average random field modelling error (in terms of  $\sigma_z$  and  $\sigma_i$ ) of the 100 synthetic surfaces generated from each seed trace (Fig. 10a) and examples of synthetic surface from seed traces WSE, X4, and Y1 (Fig. 10b, d, respectively). The modelling error is calculated as a relative error defined as the ratio of difference between the average of the 100 simulation statistics and the seed trace (average absolute error), to the value of the seed trace statistics (true value). Here, it is expressed as a percentage.

Figure 10a shows that most synthetic surfaces were generated with a relative error on the surface statistics, compared to the input statistics within a band of  $\pm 10\%$ , which Jeffery et al. (2021) deemed as acceptable. The synthetic surfaces tend to possess an average  $\sigma_z$  smaller than that of the seed trace (negative relative error), which is attributed to the local averaging process (basis of the 2D LAS algorithm), where the random field is slightly smoothed, thereby lowering the modelled  $\sigma_z$  (Casagrande 2018).

A visual comparison of the composite synthetic surface examples presented in Fig. 10b, d to the 3D digital representation of the experimental surface (Fig. 3b) suggests that the generated surfaces tend to possess more small-scale roughness than the experimental surface.

In the context of this study, the resultant roughness textures of the composite synthetic surfaces are a product of (i) the combination of random field modelling parameters (i.e., resolution, correlation length, and standard deviation of height) used to generate the daughter surfaces (here using the 2D LAS RFM) and (2) the superposition process to create the composite surface from the three daughter surfaces (refer Jeffery et al. 2021). Additionally, the observed surface roughness expression is likely to differ with employment of an alternate modelling process (refer Buzzi and Casagrande 2018) and/or random field model.

The key objective of the composite surface generation process is to create synthetic surfaces that possess distribution of gradients that are representative of the seed trace (granted within an acceptable modelling error tolerance). Therefore, if this objective is met, the visual expression of the surface is deemed not be important to the shear strength estimation process within STADSS.



**Fig. 8** Evolution of peak shear strength ( $\tau_{P\_Det}$ ) and residual shear strength ( $\tau_{R\_Det}$ ) as a function of unconfined compressive strength  $\sigma_{ci}$  (a and d), Hoek–Brown parameter  $m_i$  (b and e) and basic friction

angle  $\phi_b$  (c and f). Shear simulations conducted under initial normal stresses of 5, 14, 22, and 31 kPa

### 3.4 STADSS Predictions: Interpretation of Shear Strength Distributions

All synthetic surfaces were digitally sheared using the NDSS model and the material parameters presented in Table 1 under initial normal stresses of 5, 14, 22, and 31 kPa (as per experimental testing conditions).

Examples of the predicted peak and residual shear strength cumulative distributions for seed trace WSE, X4, and Y1 are presented in Fig. 11 (note that the horizontal scales differ between figures, but each has a range of 20 kPa). For conciseness, only results for initial normal stress 5 kPa and 31 kPa are presented, but similar results were obtained for all seed traces and initial normal stresses.

Except for peak shear strength under 31 kPa of normal stress, all distributions appear to be very steep, almost uniform, which reflects the high level of control used in the process, from the quality control of mortar and curing of specimens

to the rigorous application of random field model to produce synthetic surfaces. Visually, only the distribution of peak shear strength under 31 kPa seems to show scatter in the results, but the coefficient of variation of the results is in the order of 2%.

For natural in situ discontinuities, features that are not yet captured in the STADSS or NDSS model (e.g., mismatched surfaces, presence of infill, variable material strength, the presence of infill material, and discontinuity persistence) will introduce more uncertainty in the prediction and will result into broader distributions of shear strength, but exploration of these features is out of the scope of the present paper.

### 3.5 STADSS Predictions: Comparison of Predictions and Experimental Data

In this section, all results of shear strength presented are an average value of 100 simulations.

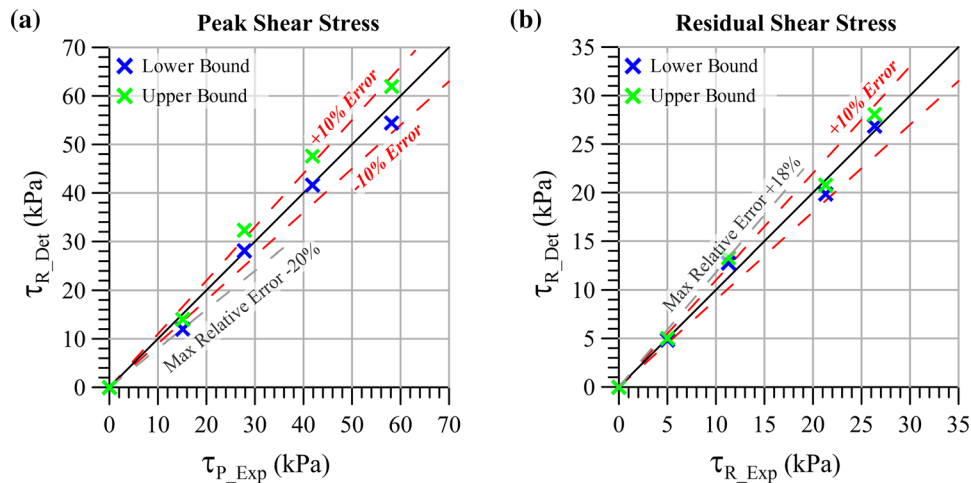


**Fig. 9** Peak and residual shear strength prediction accuracy for the upper and lower bound material cases (blue and green crosses, respectively) as a function of the experimental values for initial normal stresses ranging from 5 to 31 kPa. The continuous black line has a gradient of 1:1, red dashed lines indicate a  $\pm 10\%$  relative error and

grey dashed lines provide maximum value of relative error.  $\tau_{P\_Exp}$ : peak experimental shear strength;  $\tau_{R\_Exp}$ : residual experimental shear strength;  $\tau_{P\_Det}$ : peak deterministic shear strength;  $\tau_{R\_Det}$ : residual deterministic shear strength (Color figure online)

### 3.5.1 Predictions from a Seed Trace with Whole Surface Equivalent Statics

Figure 12a and b shows that when using a seed trace with statistics equivalent to the whole surface (WSE), the predicted peak and residual shear strength are very close to their experimental counterparts.

Figure 12a shows the STADSS tends to underestimate peak shear strength. The relative error is the highest ( $-30\%$ ) under a normal stress of 5 kPa initial normal stress, but otherwise, it is in the order of  $-10\%$ . The underestimation of shear strength is due to the relative error on gradients of all synthetic surfaces (in the order of  $-5\%$ ), as shown in Fig. 10a.

The relative error is quite small for the residual shear strength (typically within  $\pm 5\%$ ) and there is no clear tendency for underestimation or overestimation (Fig. 12b).

These results corroborate the observations of Casagrande et al. (2018), that creating synthetic surfaces from the statistics of the whole surface produces satisfactory shear strength estimates. Unfortunately, the whole surface is seldom accessible, and one has to rely on information available on a single trace.

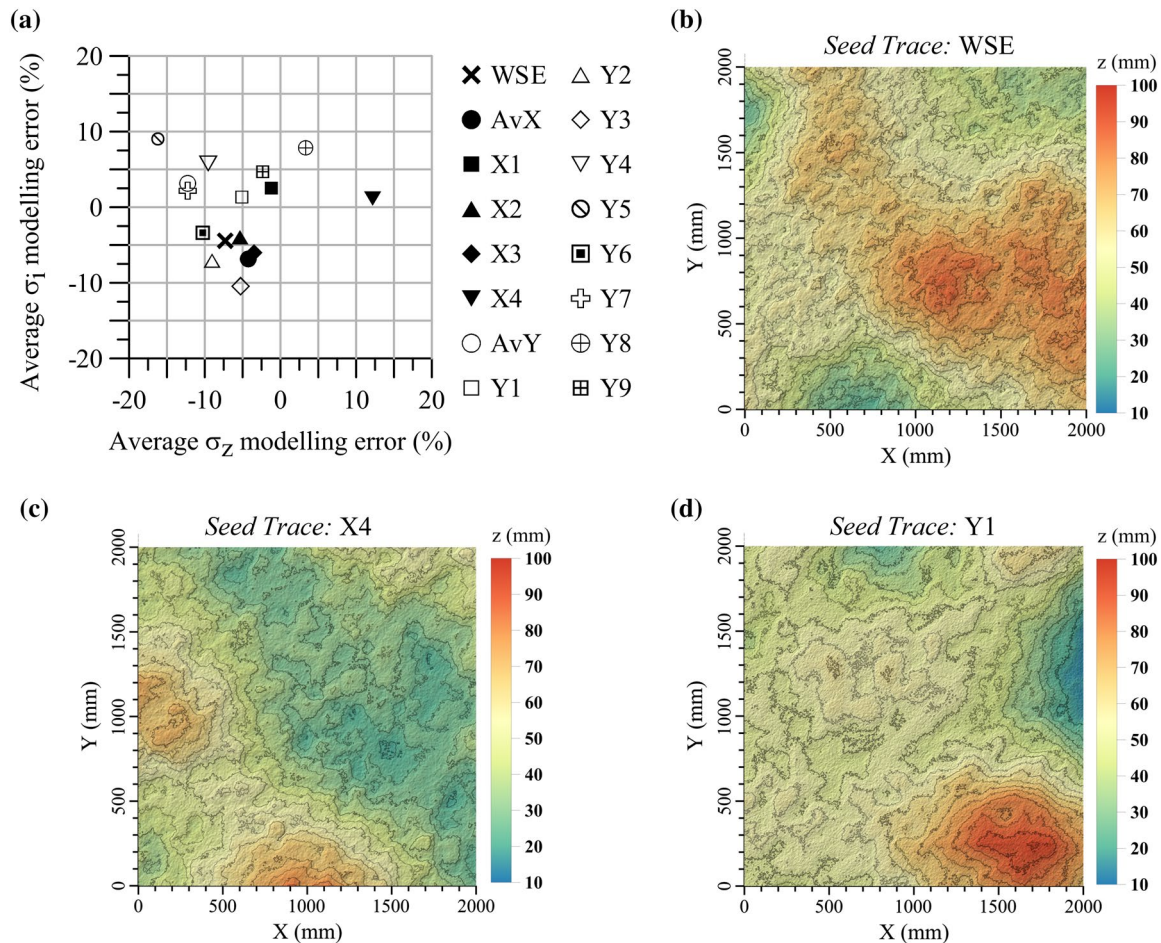
### 3.5.2 Predictions from the Statistics of a Random Seed Trace

Figure 13a–d compares experimental values of peak and residual shear strength to STADSS predictions obtained from seed traces in the X and Y directions. The first noticeable observation is the variation of predictions, ranging from

good agreement (AvX and AvY) to significant overestimations (X1 and Y4) and underestimations (X3 and Y2) with relative deviations in the order of a factor of 1.4 and 0.5, respectively. With reference to Fig. 4a and b, seed traces X1, X3, Y4, and Y2 represent the traces with the largest and smallest standard deviation of gradients  $\sigma_r$ , which in turn have produced the roughest and smoothest series of synthetic surfaces. In contrast, the prediction of residual shear strength generally shows good agreement with the experimental results, with errors typically within  $\pm 10\%$ . The predicted shear strength criteria presented in Fig. 13 confirm Buzzi and Casagrande’s (2018) view that the accuracy of stochastic shear strength predictions is strongly correlated to the gradient statistics of the seed trace and, therefore, the synthetic surfaces.

As discussed previously, the shearing direction is along Y and traces numbered X provide gradient information in the direction of shearing (traces numbered X have a constant X value and are oriented along Y, see Fig. 4). Interestingly, Fig. 13 shows that using gradient information in the direction of shearing (X traces) results in a narrower range of predictions than when using gradient information perpendicular to the direction of shearing (Y traces).

One aspect of the approach that has not been explored previously is whether the standard deviation of asperity heights  $\sigma_z$  influences the prediction of shear strength. Figure 14 presents the stochastic shear strength predictions for seed traces selected with a common  $\sigma_i$  but different  $\sigma_z$  values (see Fig. 9). Figure 14 shows that there are only minor differences between the predicted peak and residual shear strength, which can be associated with slight differences in



**Fig. 10** **a** Relative error between statistics of seed traces and statistics of synthetic surfaces generated from these seed traces, plotted in terms of standard deviation of gradients (average value computed over 100 realizations) and standard deviation of heights (average

value computed over 100 realizations); **b–d** Example of the composite synthetic surfaces generated from WSE, X4, and Y1 seed traces, respectively

the statistics of the synthetic surfaces (see Fig. 10) despite similar seed trace inputs.

### 3.6 Effect of Seed Trace Variability

One assumption of STADSS is that the seed trace used to predict shear strength is representative of the whole surface. However, Casagrande et al. (2018), Buzzi and Casagrande (2018), and this study have shown that there exists a degree of variability of asperity statistics between traces over a discontinuity surface, which Buzzi and Casagrande referred to as “seed trace variability”. Such variability of statistics is illustrated in Fig. 15, where the distributions of gradients in the X (a) and Y (b) directions are plotted. Considering the Gaussian nature of gradient distributions previously reported (Casagrande et al. 2018; Buzzi and Casagrande 2018; Jeffery et al. 2021), it is not unreasonable to assume that the distribution of all seed trace  $\sigma_i$

of the surface is also Gaussian. In fact, when superimposing theoretical normal cumulative frequency distributions to the cumulative frequency distribution of standard deviation of gradients  $\sigma_i$  for seed traces in the X and Y directions for the experimental surface (Fig. 15a and b, respectively), it shows that: 1) the experimental distributions are close to Gaussian in nature, albeit the X traces presenting with a ‘heavy tailed’ distribution and 2) there is approximately a 70% chance of selecting a seed trace with a  $\sigma_i$  that is within one standard deviation of the mean. For a Gaussian distribution, approximately 68% of the seed traces would lie within one standard deviation either side of the mean. In the rest of this section, for each direction, peak and residual shear strength have been computed from the traces indicated in Fig. 15 (AvX, X1 to X4, AvY, Y2 to Y6) to assess the sensitivity of the prediction to the input statistics.



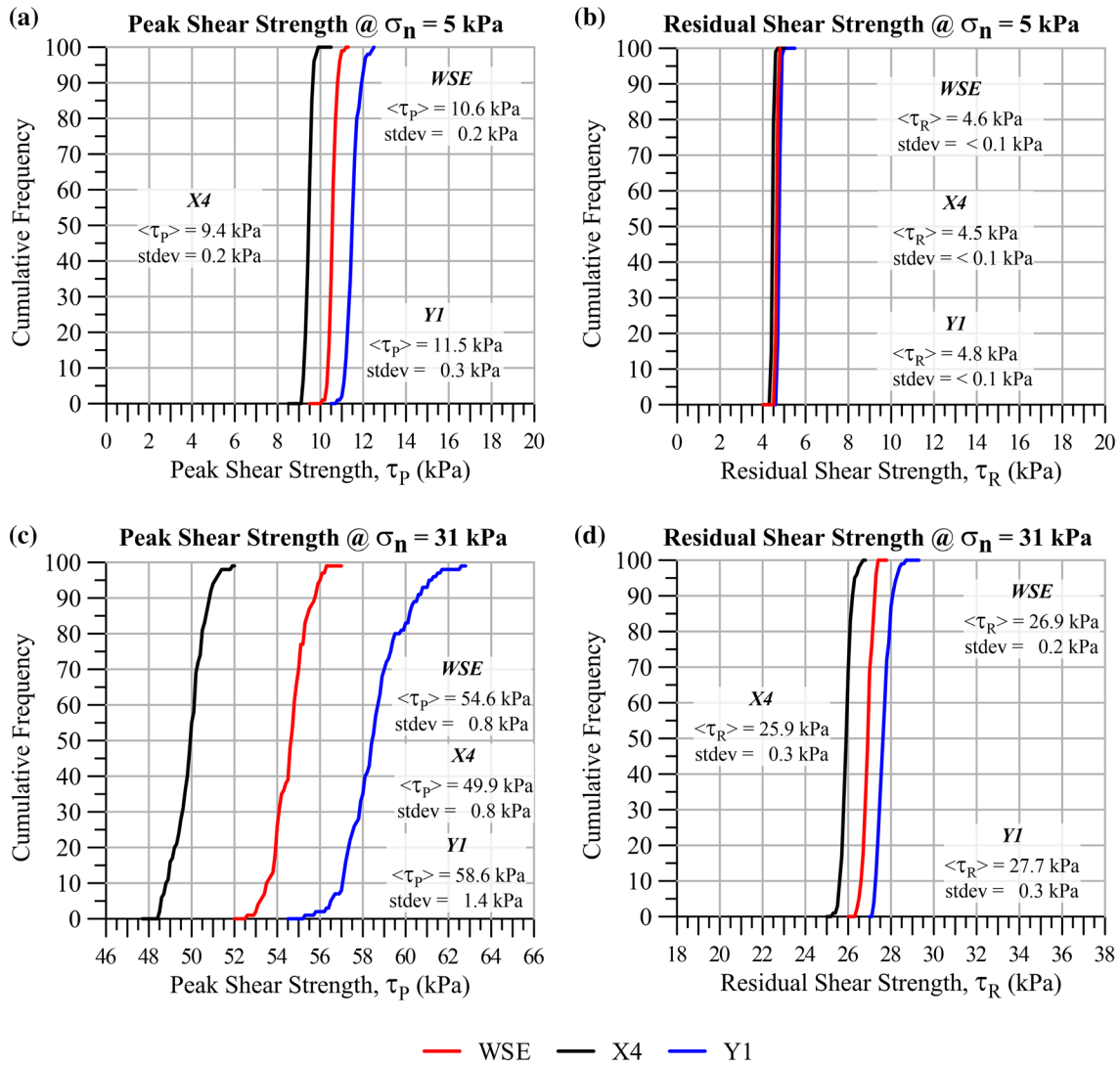


**Fig. 11** Cumulative distribution of peak shear strength under an initial normal stress of 5 kPa **(a)**; residual shear strength under an initial normal stress of 5 kPa **(b)**; peak shear strength under an initial normal stress of 31 kPa **(c)**; residual shear strength under an initial normal

stress of 31 kPa **(d)**. For each sub-figure, distributions are shown for 100 synthetic surfaces generated from traces WSE, X4; and Y1.  $\langle \tau \rangle$ : mean value of shear strength, stdev: standard deviation of shear strength

**Fig. 12** Evolution of experimental and predicted peak **(a)** and residual **(b)** shear strength as a function of applied normal stress,  $\sigma_n$ . Predictions made from a seed trace possessing statistics equivalent to the whole surface (WSE).  $\tau_{p\_Exp}$ : peak experimental shear strength;  $\tau_{R\_Exp}$ : residual experimental shear strength;  $\langle \tau_p \rangle$ : peak stochastic shear strength;  $\langle \tau_R \rangle$ : residual stochastic shear strength

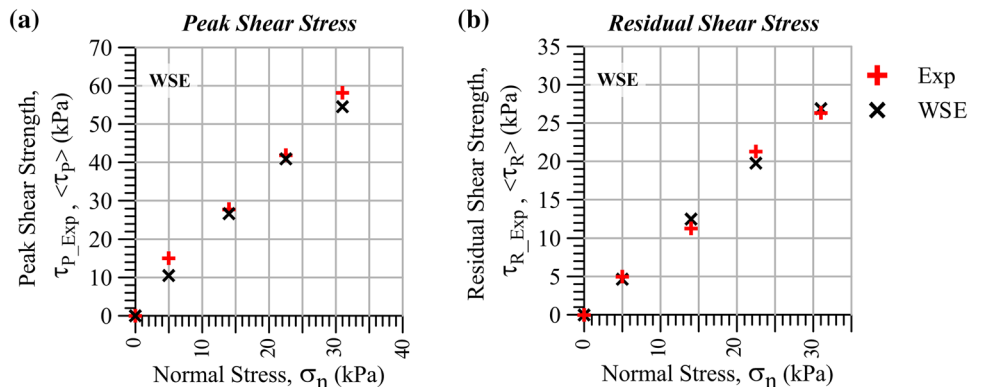


**Fig. 13** Values of experimental and predicted peak (a and c) and residual (b and d) shear strength as a function of applied normal stress,  $\sigma_n$ . Predictions made from a selection of seed traces: X traces (a and b) and Y traces (c and d).  $\tau_{P\_Exp}$ : peak experimental shear strength;  $\tau_{R\_Exp}$ : residual experimental shear strength;  $\langle \tau_P \rangle$ : peak stochastic shear strength;  $\langle \tau_R \rangle$ : residual stochastic shear strength

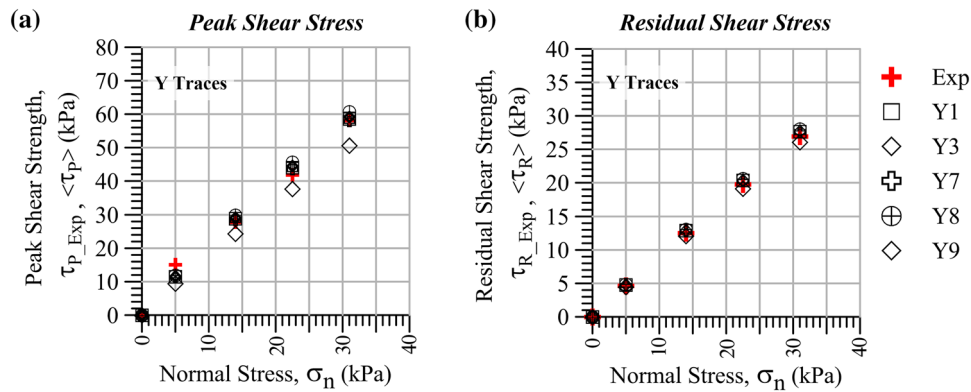
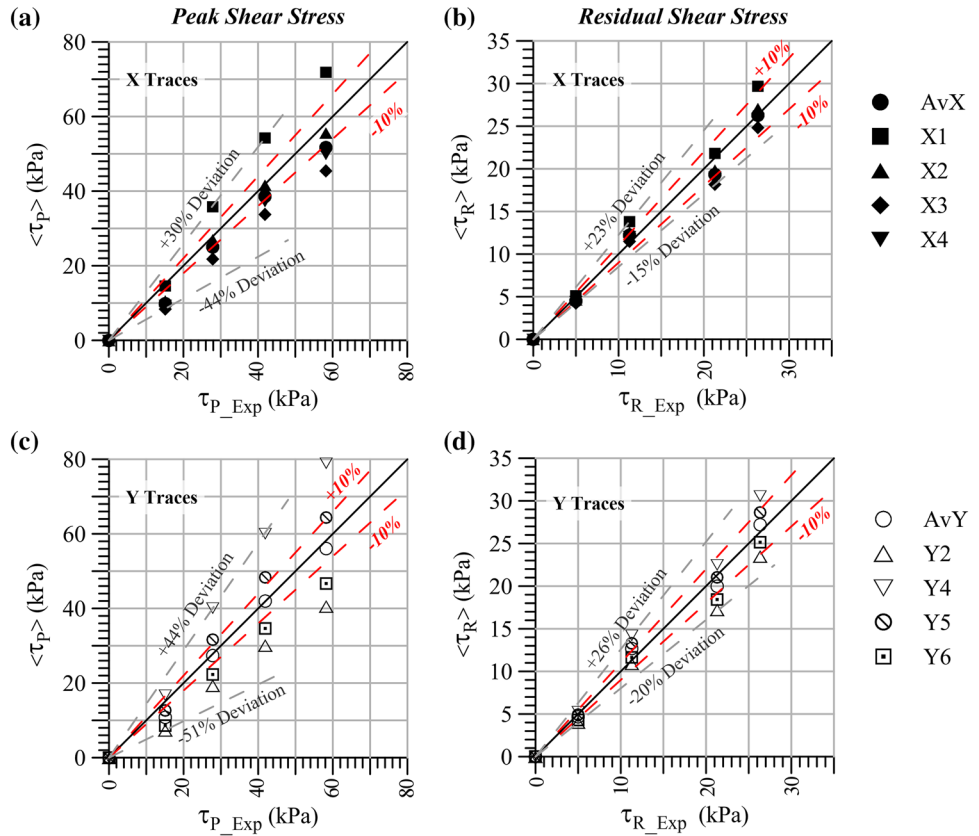


**Fig. 14** Evolution of experimental and predicted peak (a) and residual (b) shear strength as a function of applied normal stress,  $\sigma_n$ . Predictions made from Y seed traces possessing different standard deviation of heights but similar standard deviation of gradients.  $\tau_{P\_Exp}$ :

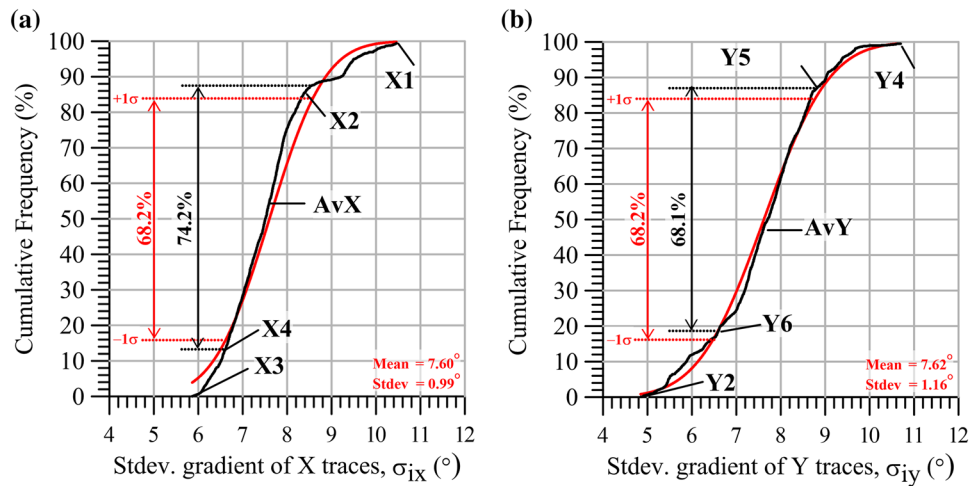
peak experimental shear strength;  $\tau_{R\_Exp}$ : residual experimental shear strength;  $\langle \tau_P \rangle$ : peak stochastic shear strength;  $\langle \tau_R \rangle$ : residual stochastic shear strength

Figure 16a and b shows how the peak and residual shear strength changes with the standard deviation of the seed trace (data for both X and Y directions are plotted in the figure). For reference, the standard deviation of the whole surface (noted WSE) and the associated shear strengths are reported as crosses in the figure. The range of standard deviation of gradients in Fig. 16a and b corresponds to the

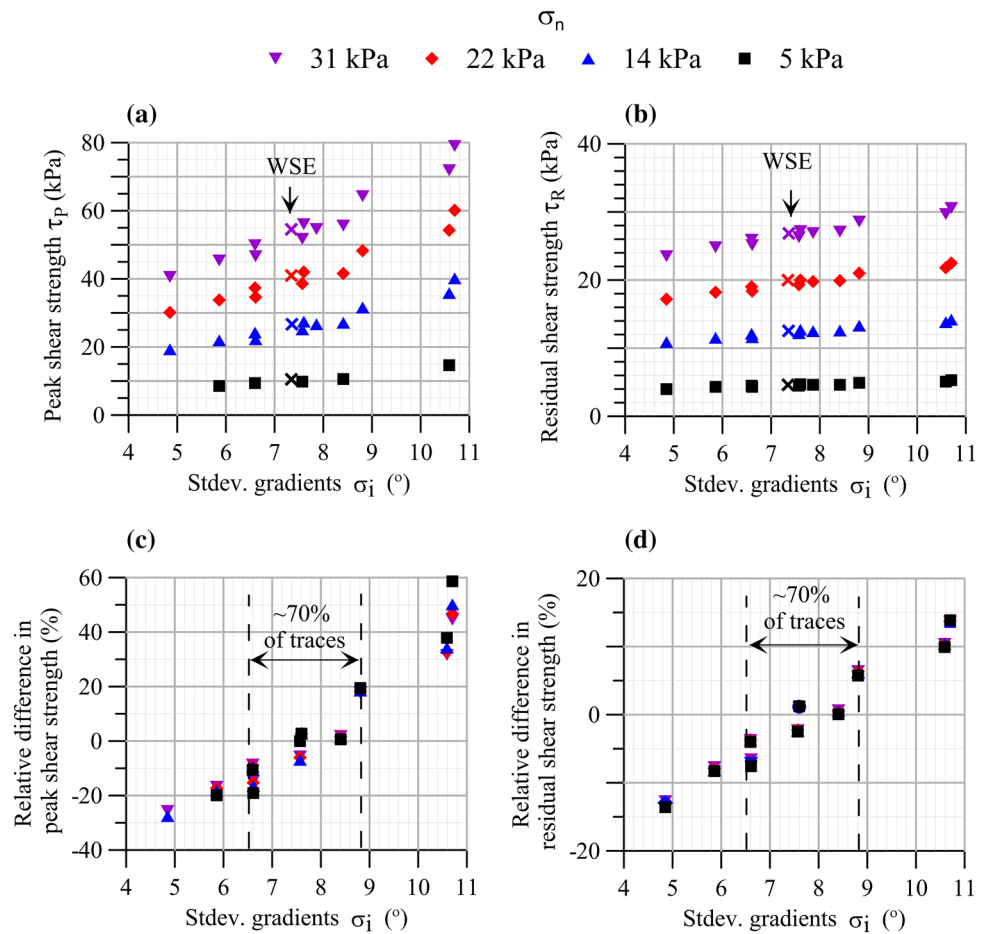
range within the surface, as indicated by the distributions of Fig. 15a and b.

The absolute difference between the shear strength at a given  $\sigma_i$  and that of the whole surface (cross WSE) increases with the difference in standard deviation of gradients between the seed trace and the surface. This suggests that the less representative of the whole surface a trace is, the poorer the prediction. The absolute difference in shear strength

**Fig. 15** Cumulative distribution of standard deviation of gradients of all X traces (a) and all Y traces (b) of the surface (black line) and equivalent theoretical Gaussian cumulative distributions (red lines) (Color figure online)



**Fig. 16** a and b Peak (a) and residual (b) shear strength as a function of the standard deviation of gradients used for the prediction for four values of normal stress. Traces in both X and Y direction were used. The coloured crosses correspond to the prediction made using statistics that are representative of the whole surface (WSE). c and d Relative difference in peak (c) and residual (d) shear strength, expressed as a percentage of the prediction made using the statistics of the whole surface, and plotted as a function of the standard deviation of gradients used for the prediction for four values of normal stress



(peak and residual) also increases with normal stress: the maximum difference in peak shear strength is 4 kPa under 5 kPa of normal stress and about 25 kPa under 31 kPa of normal stress. Finally, the difference in shear strength is less pronounced for the residual shear strength than for the peak shear strength.

When the difference is expressed as a percentage of the shear strength predicted from the statistics of the whole surface (WSE crosses in the figure), the value of normal stress becomes irrelevant (see Fig. 15c and d). In the figure, it is also indicated the range of standard deviation of gradients corresponding to  $\sim 70\%$  of traces, derived from Fig. 15. Figure 16 shows that for the surface studied, there is a 70% probability that the seed trace used for prediction will yield a relative difference in peak and residual shear strength of less than 20% and 10%, respectively.

## 4 Conclusion

This paper presents the first rigorous application of the Newcastle Discontinuity Shear Strength (NDSS) model and Stochastic Approach for Discontinuity Shear Strength (STADSS) on a 2 m-by-2 m discontinuity surface, with comparison of prediction to experimental shear strength data.

The first part of the paper presents the application of the semi-analytical NDSS model to a digital capture of the 2 m-by-2 m experimental surface. A key component of the STADSS, the efficient NDSS model, is used to process large 3D synthetic surfaces. The predictive ability of the NDSS model was found to be satisfactory, as most predictions have a relative error within a  $\pm 10\%$  range. Good agreement was also observed between the predicted and observed damage areas. A material parameter sensitivity study of the NDSS model found the prediction of the peak and residual shear strength to be sensitive to the basic friction angle parameter and the Hoek–Brown parameter  $m_i$ .

The second part of the paper presents the application of the STADSS to the 2 m-by-2 m experimental surface, with 16 seed traces selected to generate synthetic surfaces. For each seed trace, 100 synthetic surfaces were generated. Analysis of synthetic surfaces revealed that their statistics

are within  $\pm 10\%$  of the statistics of the input seed trace. The paper then examines the shear strength distributions produced by the STADSS.

The paper goes on to explore the peak and residual prediction capability of the STADSS by comparing the 16 peak and residual shear strength predictions to the available experimental data. It was observed that, for seed traces with gradient statistics equivalent to that of the surface, the predictions closely resemble the experimental results. Predicting shear strength from different seed traces results in more variability of predictions, although the majority of predictions fall within  $\pm 20\%$  of the experimental data. The predictions of residual shear strength tended to be more accurate than peak shear strength.

The variability of the asperity statistics between seed traces influences the accuracy of the stochastic prediction, which is referred to as trace variability. The paper finishes with proposing a means of quantifying the likelihood and accuracy impact that trace variability may have on the shear strength predictions. Based on the Gaussian nature of surface and seed trace gradient statistics, it is reasonable to assume that the distribution of standard deviation of gradients for all seed traces of a surface is also Gaussian. Hence, the results of this study suggest that there is a 68% chance that the observable seed trace will produce stochastic peak and residual shear strength estimates within  $\pm 20\%$  and  $\pm 10\%$  of the true strength.

The application of STADSS presented in this paper constitutes the first stage of large-scale validation. The encouraging results add merit to the overall validity of the approach for predicting the shear strength of large in situ discontinuities, in slope stability and civil infrastructure development situations where the availability of surface roughness may be limited. The authors recommend further large-scale validation, encompassing but not limited to a variety of surfaces, increase ranged of applied normal stresses, and validation context (experimental versus field application), to gain more insight on this novel approach and its possible limitations.

## Appendix A

See Tables 4 and 5.

**Table 4** Spatial increments for all daughter profiles, decoupled from the seed traces

Trace	Spatial increment (SI) for the relative scales of roughness (mm) large/intermediate/small					
	X1	X2	X3	X4	AvX	
SI <sub>L</sub> /SI <sub>I</sub> /SI <sub>S</sub>	80/20/1	200/25/1	250/50/1	200/40/1	200/40/1	
Trace	Y1	Y2	Y3	Y4	Y5	Y6
SI <sub>L</sub> /SI <sub>I</sub> /SI <sub>S</sub>	250/50/1	500/80/1	125/25/1	100/25/1	125/10/1	125/20/1
Trace	Y7	Y8	Y9	AvY	WSE	
SI <sub>L</sub> /SI <sub>I</sub> /SI <sub>S</sub>	250/50/1	100/25/1	250/50/1	250/25/1	125/40/1	



**Table 5** Summary of the random standard deviation and mean heights, correlation length, and field size for the decomposed seed trace roughness profiles

Trace	Length (mm)	Large			Intermediate			Small		
		Input statistics			Input statistics			Input statistics		
		$\sigma_z$ (mm)	$\mu_z$ (mm)	$\theta_z$ (mm)	$\sigma_z$ (mm)	$\mu_z$ (mm)	$\theta_z$ (mm)	$\sigma_z$ (mm)	$\mu_z$ (mm)	$\theta_z$ (mm)
X1	2000	256	58	460	6.2	0	57.1	0.18	0	9.4
X2	2000	228	48	670	8.2	0	84.4	0.15	0	12.4
X3	2000	257	31	1089	5.3	0	170.6	0.23	0	18.9
X4	2000	248	37	950	9.1	0	131.4	0.23	0	16.6
AvX	2000	233	34	619	6.9	0	102.8	0.24	0	16.1
Y1	2000	776	38	1218	7.7	0	157.5	0.22	0	11.6
Y2	2000	800	44	1651	7.2	0	231.8	0.29	0	27.9
Y3	2000	426	54	834	5.5	0	84.3	0.09	0	11.5
Y4	2000	481	41	695	9.1	0	76.3	0.38	0	12.2
Y5	2000	360	38	739	6.4	0	53.3	0.07	0	10.4
Y6	2000	140	49	786	3.7	0	72.6	0.07	0	10.1
Y7	2000	126	51	1057	7.1	0	98.7	0.21	0	12.9
Y8	2000	29	45	316	7.2	0	78.7	0.240	0	12.9
Y9	2000	294	49	1104	6.5	0	105.8	0.224	0	12.3
AvY	2000	268	41	985	7.4	0	121.3	0.191	0	12.1
WSE	2000	301	49	967	7.0	0	91.2	0.298	0	16.6

**Acknowledgements** The authors would like to acknowledge the financial support received from Australian Research Council via Discover Project Grant (DP190101558), Australian Government Department of Education and Training via Australian Government Research Training Program Scholarship and PSM, Sydney.

**Funding** Open Access funding enabled and organized by CAUL and its Member Institutions.

**Data availability** Data can be made available upon request, in the context of scientific collaboration.

## Declarations

**Conflict of Interest** The authors declare that they have no known competing financial interests or personal relationships that could have appeared to influence the work reported in this paper.

**Open Access** This article is licensed under a Creative Commons Attribution 4.0 International License, which permits use, sharing, adaptation, distribution and reproduction in any medium or format, as long as you give appropriate credit to the original author(s) and the source, provide a link to the Creative Commons licence, and indicate if changes were made. The images or other third party material in this article are included in the article's Creative Commons licence, unless indicated otherwise in a credit line to the material. If material is not included in the article's Creative Commons licence and your intended use is not permitted by statutory regulation or exceeds the permitted use, you will need to obtain permission directly from the copyright holder. To view a copy of this licence, visit <http://creativecommons.org/licenses/by/4.0/>.

## References

- Alejano LR, González J, Muralha J (2012) Comparison of different techniques of tilt testing and basic friction angle variability assessment. *Rock Mech Rock Eng* 45:1023–1035. <https://doi.org/10.1007/s00603-012-0265-7>
- Amarasekera DM (2015) Shear Strength Analysis for Rock Slope Stability in the Brisbane City Area. International Society for Soil Mechanics and Geotechnical Engineering. <https://www.issmge.org/publications/publication/shear-strength-analysis-for-rock-slope-stability-in-the-brisbane-city-area>. Accessed 14 Jan 2022
- Barton N (1971) Estimation of in situ shear strength from back analysis of failed rock slopes. In: *Rock Fracture: Proc of Symp of Int Soc Rock Mech Nancy*. International Society for Rock Mechanics, Paper II.27
- Barton N (1973) Review of a new shear-strength criterion for rock joints. *Eng Geol* 7(4):287–332. [https://doi.org/10.1016/0013-7952\(73\)90013-6](https://doi.org/10.1016/0013-7952(73)90013-6)
- Barton N (1976) The shear strength of rock and rock joints. *Int J Rock Mech Min Sci Geomech Abstr* 13:255–279. [https://doi.org/10.1016/0148-9062\(76\)90003-6](https://doi.org/10.1016/0148-9062(76)90003-6)
- Barton N (1982) Modelling rock joint behaviour from in situ block tests: Implications for nuclear waste repository design. Office of Nuclear Waste Isolation, Columbus, p 96 (**ONWI-308, September 1982**)
- Barton N (2013) Shear strength criteria for rock, rock joints, rock fill and rock masses: problems and some solutions. *J Rock Mech Geotech Eng* 5(4):249–261. <https://doi.org/10.1016/j.jrmge.2013.05.008>

- Barton N, Bandis S (1980) Some effects of scale on the shear strength of joints. *Int J Rock Mech Min Sci Geomech Abstr* 17(1):69–73. [https://doi.org/10.1016/0148-9062\(80\)90009-1](https://doi.org/10.1016/0148-9062(80)90009-1)
- Barton N, Bandis S (1982) Effects of block size on the shear behavior of jointed rock. In: Goodman RE, Heuze FE (eds) *Issues in Rock Mechanics: Proc 23rd US Symp Rock Mech (USRMS)*, California. Society of Mining Engineers of the American Institute of Mining, Metallurgical and Petroleum Engineers, New York. pp 739–760
- Barton N, Choubey V (1977) The shear strength of rock joints in theory and practice. *Rock Mech Rock Eng* 10:1–54. <https://doi.org/10.1007/BF01261801>
- Barton N, Wang C, Yong R (2023) Advances in joint roughness coefficient (JRC) and its engineering applications. *J Rock Mech Geotech Eng*. <https://doi.org/10.1016/j.jrmge.2023.02.002>
- Beer AJ, Stead D, Coggan J (2002) Estimation of the joint roughness coefficient (JRC) by visual comparison. *Rock Mech Rock Eng* 35:65–74. <https://doi.org/10.1007/s006030200009>
- Buzzi O, Casagrande D (2018) A step towards the end of the scale effect conundrum when predicting the shear strength of large in situ discontinuities. *Int J Rock Mech Min Sci* 105:210–219. <https://doi.org/10.1016/j.ijrmms.2018.01.027>
- Buzzi O, Casagrande D, Giacomini A, Lambert C, Fenton G (2017) A new approach to avoid the scale effect when predicting the shear strength of large in situ discontinuity. In: *Proc 70th Canadian Geotech Con, GeoOttawa 2017*, Ottawa. Canadian Geotechnical Society, Ontario, 8p
- Casagrande D (2018). A stochastic approach for the shear strength of rock discontinuities. Dissertation, University of Newcastle. <http://hdl.handle.net/1959.13/1385870>
- Casagrande D, Buzzi O, Giacomini A, Lambert C, Fenton GA (2018) A new stochastic approach to predict peak and residual shear strength of natural rock discontinuities. *Rock Mech Rock Eng* 51:69–99. <https://doi.org/10.1007/s00603-017-1302-3>
- Fardin N, Stephansson O, Jing L (2001) The scale dependence of rock joint surface roughness. *Int J Rock Mech Min Sci* 38(5):659–669. [https://doi.org/10.1016/S1365-1609\(01\)00028-4](https://doi.org/10.1016/S1365-1609(01)00028-4)
- Giani GP, Ferrero AM, Passarello G, Reinaudo L (1995) Scale effect evaluation on natural discontinuity shear strength. In: Myer LR, Tsang CF, Cook NGW, Goodman RE (eds) *Fractured and Jointed Rock Masses: Proc con on fractured and jointed rock masses*. AA Balkema Rotterdam, California, pp 447–452
- Hencher SR, Toy JP, Lumsden AC (1993) Scale dependent shear strength of rock joints. In: da Cunha AP (ed) *Scale effects in rock masses*, vol 93. CRC Press, London, pp 233–240
- Hoek E, Brown ET (1997) Practical estimates of rock mass strength. *Int J Rock Mech Min Sci* 34(8):1165–1186. [https://doi.org/10.1016/S1365-1609\(97\)80069-X](https://doi.org/10.1016/S1365-1609(97)80069-X)
- International Society Rock Mechanics (ISRM) (1983) Suggested methods for determining the strength of rock material in triaxial compression: revised version. *Int J Rock Mech Min Sci* 20(6):285–290. [https://doi.org/10.1016/0148-9062\(83\)90598-3](https://doi.org/10.1016/0148-9062(83)90598-3)
- Jeffery M, Huang J, Fityus S, Giacomini A, Buzzi O (2021) A rigorous multiscale random field approach to generate large scale rough rock surfaces. *Int J Rock Mech Min Sci* 142:104716. <https://doi.org/10.1016/j.ijrmms.2021.104716>
- Jeffery M, Crumpton M, Fityus SG, Huang J, Giacomini A, Buzzi O (2022) A shear device with controlled boundary conditions for very large nonplanar rock discontinuities. *Geotech Test J*. <https://doi.org/10.1520/GTJ20210220>
- Johansson F (2016) Influence of scale and matedness on the peak shear strength of fresh, unweathered rock joints. *Int J Rock Mech Min Sci* 82:36–47. <https://doi.org/10.1016/j.ijrmms.2015.11.010>
- Kim D, Gratchev I, Balasubramaniam A (2014) Back analysis of a natural jointed rock slope based on the photogrammetry method. *Landslides* 12:147–154. <https://doi.org/10.1007/s10346-014-0528-3>
- Kutter KH, Otto F (1990) Influence of parallel and cross-joints on shear behaviour of rock discontinuities. In: Barton N, Stephansson O (eds) *Rock Joints: Proc Int Symp on Rock Joints*, Loen. AA Balkema, Rotterdam, pp 243–250
- Leal-Gomes MJA (2003). Some new essential questions about scale effects on the mechanics of rock mass joints. In: *10th ISRM Con: Technology Roadmap for Rock Mechanics*, Sandton. South African Institute of Mining and Metallurgy, Johannesburg, pp 721–728
- Maerz NH, Franklin JA, Bennett CP (1990) Joint roughness measurement using shadow profilometry. *Int J Rock Mech Min Sci Geomech Abstr* 27(5):329–343. [https://doi.org/10.1016/0148-9062\(90\)92708-M](https://doi.org/10.1016/0148-9062(90)92708-M)
- Markov AB, Hormazabal E, Livinsky IS, Spirin VI, Soluyanov NO (2019) Methodology of back analysis of cohesion and friction of joints based on pit slope failure events. *Aust Mine Safety J* 4:95–98
- Muralha J, Grasselli G, Tatone B, Blumel M, Chryssanthakis P, Yujing J (2013) ISRM suggested method for laboratory determination of the shear strength of rock joints: revised version. *Rock Mech Rock Eng* 47:291–302. <https://doi.org/10.1007/s00603-013-0519-z>
- Muralha J, Pinto Da Cunha A (1990a) About LNEC experience on scale effects in mechanical behaviour In: Pinto da Cunha A (ed). *Scale Effects in Rock Masses: Proc 1st Int Workshop on Scale Effects in Rock Masses*, Loen. A.A. Balkema, Brookfield, pp 131–147
- Muralha J, Pinto da Cunha A (1990b). Analysis of scale effects in joint mechanical behaviour. In: Pinto da Cunha A (ed). *Scale Effects in Rock Masses: Proc 1st Int Workshop on Scale Effects in Rock Masses*, Loen. A.A. Balkema, Brookfield, pp 191–200.
- Ohnishi Y, Yoshinaka R (1995) Laboratory investigation of scale effect in mechanical behaviour of rock. In: Myer LR, Tsang CF, Cook NGW, Goodman RE (eds) *Fractured and Jointed Rock Masses: Proc con on fractured and jointed rock masses*, California. AA Balkema, Rotterdam, pp 465–470
- Pratt HR, Black AD, Brown WS, Brace WF (1972) The effect of specimen size on the mechanical properties of unjointed diorite. *Int J Rock Mech Min Sci Geomech Abstr* 9(4):513–516. [https://doi.org/10.1016/0148-9062\(72\)90042-3](https://doi.org/10.1016/0148-9062(72)90042-3)

**Publisher's Note** Springer Nature remains neutral with regard to jurisdictional claims in published maps and institutional affiliations.